Additive Manufacturing 116 (2026) 105083

Contents lists available at ScienceDirect

Additive Manufacturing

journal homepage: www.elsevier.com/locate/addma

Synergistic effects of etching and electropolishing on additively manufactured Ti-6Al-4V scaffolds for biomedical implants

Ruben del Olmo [a,*], Reynier I. Revilla [a], Floriane Debuisson [b], Kitty Baert [a], Brecht Van Hooreweder [c], Anne des Rieux [b], Iris De Graeve [a], Ana Santos-Coquillat [b,*]

[a] Department of Materials and Chemistry, Research Group of Sustainable Materials Engineering (SUME), Vrije Universiteit Brussel (VUB), Brussels 1050, Belgium
[b] Université catholique de Louvain, UCLouvain, Louvain Drug Research Institute, Advanced Drug Delivery and Biomaterials, Avenue E. Mounier 73, Brussels 1200, Belgium
[c] Department of Mechanical Engineering, KU Leuven, Celestijnenlaan 300b, Leuven B 3001, Belgium

ARTICLE INFO

Keywords:
Titanium
Additive manufacturing
Etching
Electropolishing
Stem cells
Biomedicine

ABSTRACT

Additive manufacturing (AM) of Ti alloys, particularly for complex-shaped prosthetics in biomedicine, offers a promising solution for improving biomaterial applications in the human body. However, as-printed titanium alloys often present defects, such as partially molten particles and surface heterogeneities, which can hinder implant integration and cell-material interactions. This study investigates, for the first time, the impact of two surface treatments combined - chemical etching and electropolishing - on a scaffold-shaped Ti-6Al-4V alloy fabricated via laser powder bed fusion. While neither treatment achieved an optimal finish, their combination (etching + electropolishing) significantly reduced surface roughness and promoted a thicker, more homogeneous TiO_2 layer, resulting in a surface free of unmelted particles and a smooth finish. The materials were biocompatible with stem cells from the apical papilla (SCAP) in direct contact assays. While all scaffolds supported cell viability, the surface-modified candidate allowed a monolayer formation after 15 days in contact with the cells. Also, when seeded onto the material, an enhanced tissue-like matrix development was found after 28 days. An increased expression of CD90 and a conserved expression of CD73 and CD105 (positive stem cell markers) were observed after 28 days of culture, whereas osteogenic differentiation markers (Collagen I, alkaline phosphatase, and Runx2) were also increased, presenting a mixed population within the 3D structure. Additionally, no signs of oxidative stress were observed after 24 h with macrophages. These results demonstrate that combining etching and electropolishing for AM Ti alloys is a promising strategy for enhancing the biomedical performance of 3D-printed Ti alloys.

1. Introduction

Additive manufacturing (AM) technology has been applied in prosthetic design or scaffolds for tissue engineering (TE), as it can reduce human body rejection of biomaterials [1]. Unlike conventional processing methods, AM allows freedom of design, customization, and more importantly, reproduction of complex geometries that can be obtained from the patient by Digital computer-aided (CAD) design [2]. In this context, metal additive manufacturing (MAM), particularly for titanium (Ti) alloys, has increasingly become a cutting-edge technology in prosthetics to print patient-specific mold-free 3D complex-shaped structures with precise control. Moreover, traditional Ti prostheses present a higher elastic modulus when compared to human bone, resulting in stress shielding that can lead to aseptic loosening and implant failure. For these reasons, there is a need for new Ti prostheses with similar mechanical performance to human bone [3,4]. Nevertheless, although this technology has meant a turning point in material science, several challenges for clinical translation persist, especially those regarding surface quality, mechanical reliability, cell compatibility, and implantability [5–7].

A critical first step to address the abovementioned limitations is the careful selection of an appropriate MAM technology. The choice of MAM technique directly influences the microstructure, surface topography, and mechanical performance of titanium implants. These features, in turn, affect biological responses such as cell adhesion, proliferation, and osteointegration. Selecting a process that balances geometric precision,

* Corresponding authors.
E-mail addresses: Ruben.Del.Olmo.Martinez@vub.be (R. del Olmo), ana.santos@uclouvain.be (A. Santos-Coquillat).

https://doi.org/10.1016/j.addma.2026.105083
Received 18 June 2025; Received in revised form 26 November 2025; Accepted 5 January 2026
Available online 6 January 2026

control over porosity, and surface finishing is essential to maximize the clinical performance of patient-specific implants and to provide a reliable foundation for subsequent surface treatments or modifications [8,9].

So far, the most widely addressed MAM technologies in prosthetics are Electron Beam Melting (EBM) and Laser Engineered Net Shaping (LENS), a laser-based Directed Energy Deposition technique. These technologies have been explored primarily using Ti-6Al-4V, a particularly relevant material in orthopedic and dental applications due to its high strength-to-weight ratio, excellent corrosion resistance, biocompatibility, and proven clinical performance [9]. Namely, EBM-produced Ti6Al4V implants have shown improved mechanical performance compared to cast implants and present hydrophilic surfaces that promote protein adhesion and osteointegration, which is critical to accelerate the early-stage bone healing in dental applications [10,11]. Similarly, LENS, although intended for orthopedic implants, allows tailoring implant porosity and elastic modulus to values close to cortical bone, reducing stress shielding and enhancing tissue growth and vascularization [12,13].

Notwithstanding, although EBM and LENS have shown promising results, their limitations in surface resolution and the need for post-processing have led powder bed fusion (PBF) techniques - particularly laser powder bed fusion (LPBF) - to consolidate as a feasible candidate. In detail, LPBF shows superior geometric resolution, higher surface quality, and greater reproducibility in processing Ti-6Al-4V and other Ti-based alloys [14–17]. These features are particularly relevant for oral implantology, where precision, surface-controlled osseointegration, and long-term mechanical reliability are critical factors to take into account.

However, the inherent characteristics of the LPBF process introduce surface-related limitations, including uncontrolled surface roughness, residual stress, porosity, and the presence of unmelted particles, which can compromise the mechanical integrity and long-term performance of implants. Given these limitations, the design of titanium structures must consider key parameters such as porosity, surface chemistry, and roughness, which play a critical role in cell attachment, proliferation, and differentiation, thus directly affecting their osseointegration potential [18,19]. In this scenario, although optimizing printing parameters is essential to minimize these defects, most surface issues remain intrinsic to the AM process [15,20].

Therefore, to enhance the long-term performance of additively manufactured Ti alloys, surface treatments are essential to modulate surface topography and chemistry, which directly influence cell-material interaction and osteogenesis [8,21,22]. Among the numerous mechanical and physical approaches available, chemical and electrochemical treatments have proven to be particularly effective, simple, and cost-effective [23,24]. On this basis, the two most prominent and recent chemical/electrochemical approaches include (i) chemical etching with aqueous mixtures of hydrofluoric/nitric (HF/HNO_3) acids, which mitigates the risk of hydrogen embrittlement using stand-alone HF, and (ii) electropolishing for reducing roughness and homogenizing the surface [8,23]. However, conventional acidic/organic-based electropolishing electrolytes raise environmental concerns [25,26]. In this regard, recent approaches include electropolishing in eco-friendly electrolytes, such as inorganic salts and conventional organic solvents, achieving an effective roughness reduction without significantly compromising the mass loss of the component [26].

To date, to the best of the author's knowledge, most studies investigating surface treatments for LPBF-manufactured Ti alloys have primarily focused on mechanical properties - an essential but insufficient criterion - for biomedical applications. Besides, the implementation of surface treatments in complex-shaped LPBF-printed Ti alloys and their evaluation as biomaterial remains scarcely explored [22,27]. Furthermore, the use of clinically relevant cells, such as stem cells, is also limited in these studies.

To take a step forward, the ultimate goal of this study is to develop a cost-effective, eco-friendly, and simple surface treatment to enhance the surface finish and implantability of LPBF-manufactured Ti-6Al-4V scaffolds. Namely, a screening of chemical etching and electropolishing conditions was performed, followed by surface characterization via SEM and preliminary biocompatibility tests. The most promising treatments were combined and assessed with human Stem Cells From the Apical Papilla (SCAP) as a therapeutically relevant *in vitro* model. Scaffold-shaped structures were evaluated for their high relevance for biomedical applications, offering an advantageous lightweight/strength combination.

2. Materials and methods

2.1. LPBF printing Ti-6Al-4V scaffold

The LPBF Ti6Al4V scaffolds were produced using a Concept Laser Mlab machine with a 100 W IPG fiber laser having a wavelength of 1064 nm and a 35 μm spot size, using Carpenter Ti6Al4V fine powder with d50 = 45 μm. A layer thickness of 30 μm was used, with laser power 42 W, scanning speed 300 mm/s, and hatch distance and contour offset of 77 μm. Two contours and then one fill were used with zig-zag scanning and 90° inter-layer rotation. 8 scaffold-shaped structures were fabricated with dimensions of 15 × 15 x 20 mm^3 containing diamond unit cells with unit cell size of 1,5 × 1,5 × 1,5 mm^3 and with relative density of 43 ± 3 %. No post-heat treatments were applied to the studied scaffolds. The scaffolds selected for biomedical evaluation were cut mechanically into pieces of approximately 15 × 20 x 3 mm^3 (pictorially represented in Fig. 1).

2.2. Etching and electropolishing of the LPBF-printed Ti-6Al-4V scaffold

Before the surface modification, the as-printed Ti-6Al-4V scaffolds were ultrasonically cleaned in ethanol for 5 min and dried under an air stream.

For etching, two HF/HNO_3 ratios have been tested: 20 v.% HNO_3/1.5 v.% HF and 20 v.% HNO_3/2.2 v.% HF. The choice of 20 v.% HNO_3/2.2 v.% HF is based on the reported active titanium dissolution process. The 20 v.% HNO_3/1.5 v.% HF solution has been shown to dissolve the matrix without passivating the surface [28,29]. In both cases, three times (5, 10, and 15 min) were tested to evaluate their performance in removing unmelted particles and improving surface smoothing.

The electropolishing process was performed using a power supply (ES 0300–0.45; Delta Elektronika) connected to a two-electrode cell configuration, where the scaffold acted as the working electrode and a platinum electrode as the cathode. The electrolyte was composed of 0.25 M NaCl dissolved in 100 mL of water and ethylene glycol to a final volume of 1 liter. For the optimization process, different voltages (25–100 V) and treatment times (2–60 min) were tested at a constant stirring rate (500 rpm) and temperature (22.5 °C). After etching and/or electropolishing, the scaffolds were rinsed several times in distilled water, ultrasonically cleaned in ethanol for 10 min, dried with air, and stored in a desiccator for at least 24 h before further evaluation.

The mass loss was calculated by weighing the difference between the scaffold weight before and after each surface treatment. For clarity, only the average mass loss values were plotted as the standard deviation of the measurements was less than 10 % of the average in all treatments. The detailed data are shown in Supplementary Figure S1.

2.3. Microstructural characterization of the LPBF-printed Ti-6Al-4V scaffolds

The roughness of the scaffolds (R_a: arithmetic mean value in a roughness profile) was assessed using a Leica DMi8 optical microscope, equipped with Leica Application Suite X software. For this purpose, the image stacking mode was used to acquire a series of images at different focal depths, enabling accurate reconstruction of the surface topography and generation of roughness profiles. An average of 10 profiles in

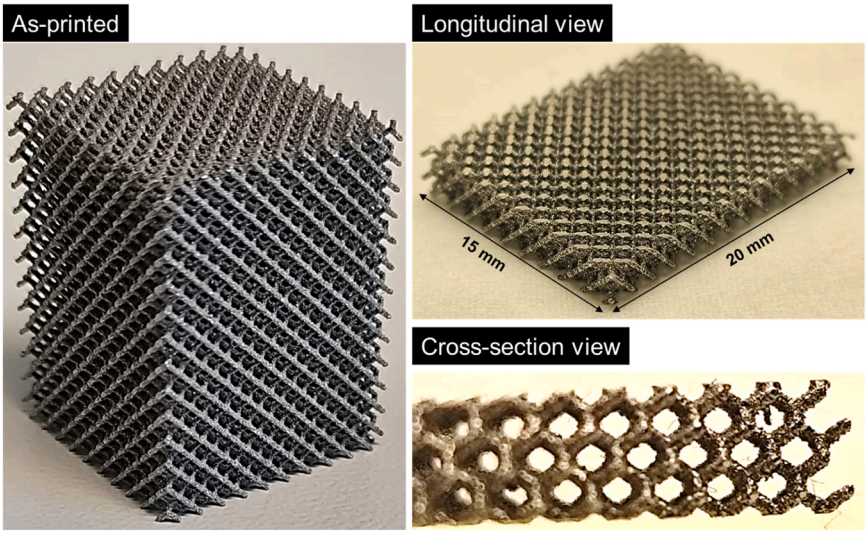

Fig. 1. The scaffold structure of the studied LPBF Ti-6Al-4V scaffold.

different locations were analyzed for each sample type, both before and after the selected surface treatments. Note that R_a values have been obtained from flat-shaped samples.

The microstructural characterization of the as-printed and surface-treated scaffolds was carried out by scanning electron microscopy (SEM; JEOL JSM-7100F) and energy-dispersive X-ray spectroscopy (EDS).

The elemental composition of the passive oxide layer of flat Ti scaffolds was studied using X-ray photoelectron spectroscopy (XPS). XPS spectra were collected using a VersaProbe III photoelectron spectroscope (Physical Electronics) with an Al Kα monochromatic X-ray source (1486.71 eV of photons). The vacuum in the analysis chamber was approximately 10^{-6} Pa during measurements. High-resolution scans of the Ti 2p, O 1 s photoelectron peaks were recorded from a spot diameter of 100 μm using a pass energy of 26 eV and a step size of 0.1 eV. Measurements were performed with a take-off angle of 45° with respect to the scaffold surface. Data was analyzed with Multipak software. The energy scale of the XPS spectra was calibrated relative to the binding energy of Ti 2p3/2 (458.5 eV) in Ti (IV). Note that all the spectra have been obtained from flat samples.

2.4. Electrochemical evaluation of the LPBF-printed Ti-6Al-4V scaffolds

Potentiodynamic polarization experiments were carried out using a Metrohm Autolab PGSTAT302N potentiostat/galvanostat with the sample as the working electrode, a saturated Ag/AgCl reference electrode, and a platinum counter electrode. The used electrolyte was α-MEM medium (Sigma-Aldrich, St Louis, USA) at room temperature. Measurements were performed after 1 h of immersion to allow stabilization, and the open circuit potential (OCP) at that time was used as the starting potential. The potential was scanned anodically from 0.1 V below OCP to 1.5 V above OCP at 0.1 $V \cdot min^{-1}$. Three curves were recorded for each sample (~1 cm^2).

2.5. Biomedical evaluation of LPBF-printed Ti-6Al-4V scaffolds

2.5.1. Cell culture

The stem cells used for this study were isolated from the human apical papilla of immature permanent teeth and fully characterized (RP89 cells) [30] – following Belgian regulations, cells were registered in UCLouvain Biobank (BB190051). GFP (Green Fluorescent Protein) expressing SCAP cells were obtained by lentivirus transduction with the TM914 vector [31,32]. The transduction and lentivirus stock production were kindly performed in the Michiels' lab (de Duve Inst., UCLouvain, Belgium) as described in [33]. Cells were cultured at 37°C, in humidified conditions at 5 % CO_2 with α-minimum essential medium (α-MEM; Sigma-Aldrich, St Louis, USA) supplemented with 10 % (V/V) fetal bovine serum (FBS, Sigma-Aldrich, St Louis, USA) and 1 % (V/V) antibiotic solution (Pen Strep, Gibco, NY, USA). Upon confluency of ~80 %, cells were passaged by detaching with StemPro™ Accutase® (Gibco, NY, USA) and washed using Dulbecco's phosphate-buffered saline (DPBS, Gibco, NY, USA). Human SCAP with passage numbers 8– 9 were used.

2.5.2. Biocompatibility

GFP+ cells were seeded at a density of 10.000 cells/cm^2 into 12 well plates, allowed to form a monolayer for 72 h, and titanium scaffolds were placed in contact with the cells following the ISO 10993 standard. Briefly, titanium scaffolds (As printed, Etched, Etched+Electropolished) were sterilized three times with 70 % EtOH for 24 h, followed by 3x DPBS and 1x α-MEM washes, before being deposited on the cell monolayer.

SCAP metabolic activity was assessed using the PrestoBlue assay (ThermoFisher Scientific) at 24 h, 96 h, and 7 days of scaffold incubation with the cells according to the supplier's instructions (n = 3–4).

Additionally, cells were allowed to grow in contact with the scaffolds for 15 days. Cells were then fixed with paraformaldehyde (PFA) 4 vol% for 10 min, washed with DPBS, permeabilized with 0.05 % Triton X-100, stained with DAPI (1:1000) and Rhodamine Phalloidin (1:1000; Abcam, UK) for 40 min. Fluorescent microscopy was used to identify cells in the green channel (488 nm) due to the SCAPs' intrinsic GFP fluorescence, nuclei in blue (405 nm), and actin in orange (555 nm) (Axiovert 200 M, Zeiss). For SEM examination, scaffolds were dehydrated with subsequent ethanol gradients (40, 50, 60, 70, 80, and 90 %) for 10 min each. Before imaging, scaffolds were coated with a 3 nm gold layer by sputtering (Cressington sputter coater-208HR). SEM (JEOL JSM-7100F) was used with a 5 kV acceleration for cell observation.

Lastly, non-fluorescent SCAP cells were seeded on top of the materials at a cell density of 100,000 cells per scaffold, allowed to adhere and grow, and a live/dead assay was performed at 24 h and 96 h. Cells were stained with Calcein-AM (1 μM) and Ethidium Homodimer (4 μM) for 1 h. Samples were analyzed by fluorescence microscopy using an LSM-980 Multiphoton confocal (ZEISS). Z-stacks were acquired - Calcein-AM was purchased from Biotium (Fremont, CA, USA) - Ethidium homodimer D-1 (EthD-1) was purchased from Invitrogen, Thermo Fischer Scientific (Waltham, MA, USA).

2.5.3. ROS determination in RAW 264.7 macrophages

Following the manufacturer's instructions, a cellular ROS assay kit

(Abcam) was used to measure intracellular ROS levels of cells in contact with the scaffolds. RAW 264.7 murine macrophages (75,000 cells) in α-MEM Phenol Red free medium (FBS 10 %), were incubated overnight with scaffolds As-printed or Etched +Electropolished (n = 4). As a positive control, TBHP (100 μM) was used as an oxidative stress inducer and was added 1 h before staining. Scaffolds were removed before DCFDA staining. Cells were stained with DCFDA (20 μM) for 45 min. Fluorescence (Ex/Em 485/535 nm) was measured using a SpectraMax ID5 (Molecular Devices). ROS response was expressed relative to the negative control. Cells were imaged with an inverted fluorescent microscope for DCF signal in green (Axiovert 200 M, Zeiss).

2.5.4. Characterization of SCAP growth on the LPBF-printed Ti-6Al-4V scaffolds

GFP+ SCAP cells were seeded on as-printed and Etched + Electropolished (Et EP) scaffolds and cultured for 28 days in regular medium. For each scaffold (size: 75 ×75 mm), 200,000 cells were seeded. Cell culture medium was changed every 2–3 days, and cell growth was monitored by wide-field microscopy (AMEX1000: EVOS™ XL Core Imaging System) at 7, 14, 21, and 28 days and with fluorescent microscopy (Axiovert 200 M, Zeiss) (SCAP intrinsic GFP signal) at 8, 15, and 25 days. After this time, for SEM imaging, scaffolds were fixed with PFA 4 % for 10 min, washed with DPBS, and dehydrated with subsequent ethanol gradients as described in Section 2.5.2.

Total RNA from SCAP (n = 4) was extracted using TRIzol™ reagent (Thermo Fisher Scientific) according to the manufacturer's instructions. SCAP-GFP^{+} cells (same passage) were used as a control, together with a 2D control of cells growing for 28 days. Reverse transcription was performed using the GoScript Transcription System (Promega, Madison, USA) from 1 μg of total RNA. qPCR was performed with qPCR Master Mix (Promega) and a STEPone PLUS instrument and software (Applied Biosystems, Foster City, USA). Data were analyzed with the ΔΔCt method using the 60S ribosomal protein L13 (RPL13) as a reference gene. Primer sequences are given in Table 1.

2.5.5. Statistical analysis

Data were analyzed using Prism software 10.4.1 (Graph pad, Inc.). A Shapiro–Wilk test was performed to confirm the normality of the distribution in the groups after performing a Grubbs outlier test. The statistics assessment was performed for PrestoBlue results using two-way ANOVA followed by Dunnett's multiple comparisons test. PCR results were analyzed using one-way ANOVA followed by Tukey's multiple comparison test (parametric). Compact Letter Display (CLD) was used to indicate significant differences between scaffolds. Data are represented as mean ± standard error of the means (SEM), and a p-value less than 0.05 was considered statistically significant.

3. Results and discussion

3.1. Optimization of etching and electropolishing parameters on LPBF Ti-6Al-4V scaffolds

To evaluate the effectiveness of chemical etching and electropolishing post-treatments in removing unmelted particles while minimizing structural degradation and material loss, various conditions were tested on Ti-6Al-4V scaffolds. In detail, Fig. 2 shows the surface morphology of Ti-6Al-4V scaffolds after etching and electropolishing, along with 3D mass loss diagrams under the studied conditions.

Regarding the etching process (Fig. 2A), the lower HNO_3:HF ratio (20:1.5) barely dissolved the unmelted particles at the studied times. In contrast, the higher HNO_3:HF ratio (20:2.2) effectively removed most particles within 15 min, along with some scaffold material. As expected, this condition also led to the highest mass loss (~25 wt% after 15 min of treatment) among all tested conditions (Fig. 2B). This behaviour aligns with previous studies showing that low $[F^-]/[NO_3^-]$ ratios in the etching solution ($\leq$ 0.1) promote Ti passivation rather than its dissolution [34,35]. Additionally, scaffold dissolution is influenced by its size, as etching efficiency has also been reported to be governed by the molar ratio between fluoride anions (F^-) and dissolved titanium [29,35].

It is worth mentioning that the successful removal of unmelted particles was consistently observed on both external and internal surfaces, thus confirming the etching efficiency throughout the scaffold geometry. Nonetheless, from a critical and technological perspective, given the relatively small size of the scaffolds, further research is needed to address the applicability and effectiveness of these treatments in larger scaffolds.

By contrast, although none of the electropolishing conditions (Fig. 2C) completely removed the unmelted particles, a noticeable smoothing effect was achieved at higher voltages ($\geq$ 50 V), particularly at 100 V for 2 min, which in turn showed the lowest mass loss (Fig. 2D). An interesting feature of this condition is the appearance of a slightly blue coloration on the surface (Figure S1), which is usually associated with the thickening of the TiO_2 oxide layer [25,36]. This observation contrasts with findings from several studies, which report that Ti electropolishing Cl-containing ethylene glycol solutions leads to the formation of a brown surface layer composed of titanium tetrachloride ($TiCl_4$) and titanium ethoxide ($C_8H_{20}O_4Ti$) [26,37]. It is also worth noting that these Ti electropolishing procedures operate at lower voltages (20–25 V) than those of the present study (25–100 V). Therefore, in the present study, the absence of this brown-colored layer in the electropolished scaffolds suggests that, although it may have initially formed, it was likely hydrolyzed [26].

Based on these findings, it can be concluded that the electropolishing process alone was insufficient to reduce surface roughness and remove unmelted particles. Therefore, the following section presents a detailed characterization of the microstructure and the TiO_2 oxide layer formed using the combined approach of chemical etching (HNO_3/HF: 20/2.2 for 15 min) and electropolishing (100 V for 2 min), referred to as the "etched + electropolished" method. The as-printed and etched (HNO_3/

Table 1
List of primer sequences.

Gene	Forward (5′-3′)	Reverse (5′-3′)
Human RPL13	CATAGGAAGCTGGGAGCAAG	GCCCTCCAATCAGTCTTCTG
Human Col1	CACCAATCACCTGCGTAGAG	AGATCACGTCATCGCACAAC
Human CD90	ACTGCCGCCATGAGAATACC	CTGGTGAAGTTGGTTCGGGA
Human CD73	CCTGAGACACACGGATGAAA	ATGCTCAAAGGCCTTCTTCA
Human CD105	GCATCACCTTTGGTGCCTTC	AACGCGTGTGCGAGTAGAT
Human CAT	GGGTCCCGAACTGTGTCA	CCATCGCAGTTCGGTTCT
Human ALPL	GACAAGAAGCCCTTCACTGC	AGACTGCGCCTGGTAGTTGT
Human Runx2	CCCTCGGAGAGGTACCAGA	TTGGGGAGGATTTGTGAAGA
Human OCN	GGCAGCGAGGTAGTGAAGAG	CCTGAAAGCCGATGTGGT
Human TSG6	TCAAGTATGGTCAGCGTATTCACC	CACAGTATCTTCCCACAAAGCCA

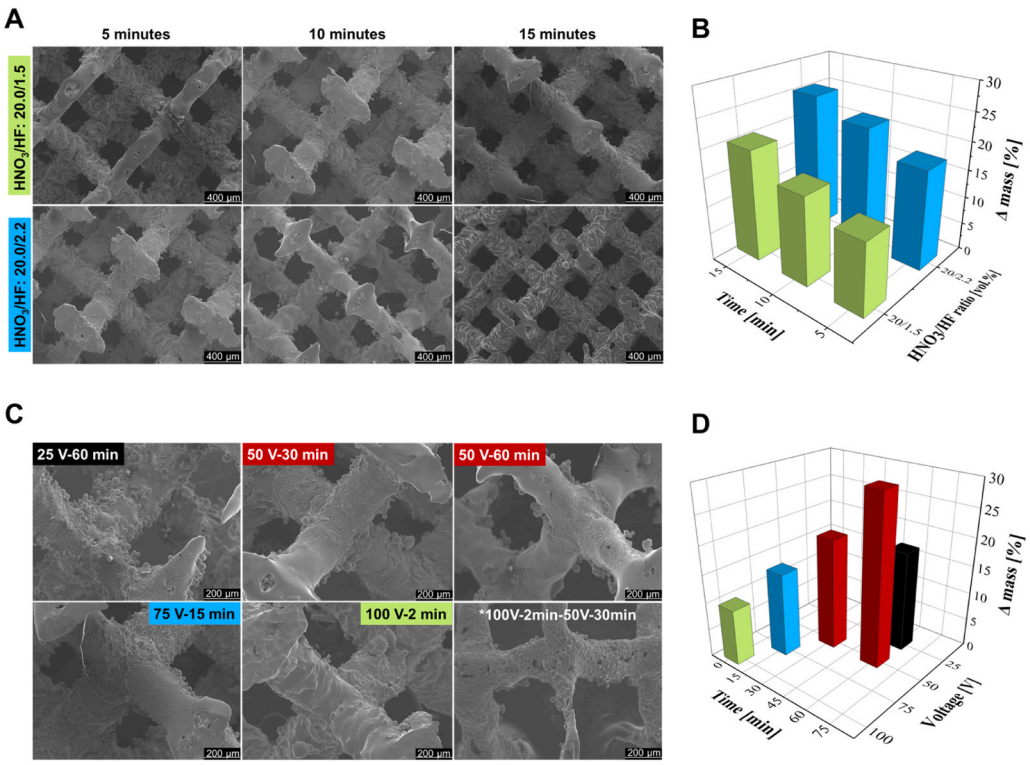

Fig. 2. Screening process to achieve the best treatment conditions. Scanning electron micrographs and mass loss of as-printed LPBF Ti-6Al-4V scaffolds after (A) etching and (C) electropolishing surface treatments with their corresponding mass-loss diagrams (B, D). The results are based on a sample size of n = 4 per condition (Table S1).

HF: 20/2.2 for 15 min) scaffolds are included as controls.

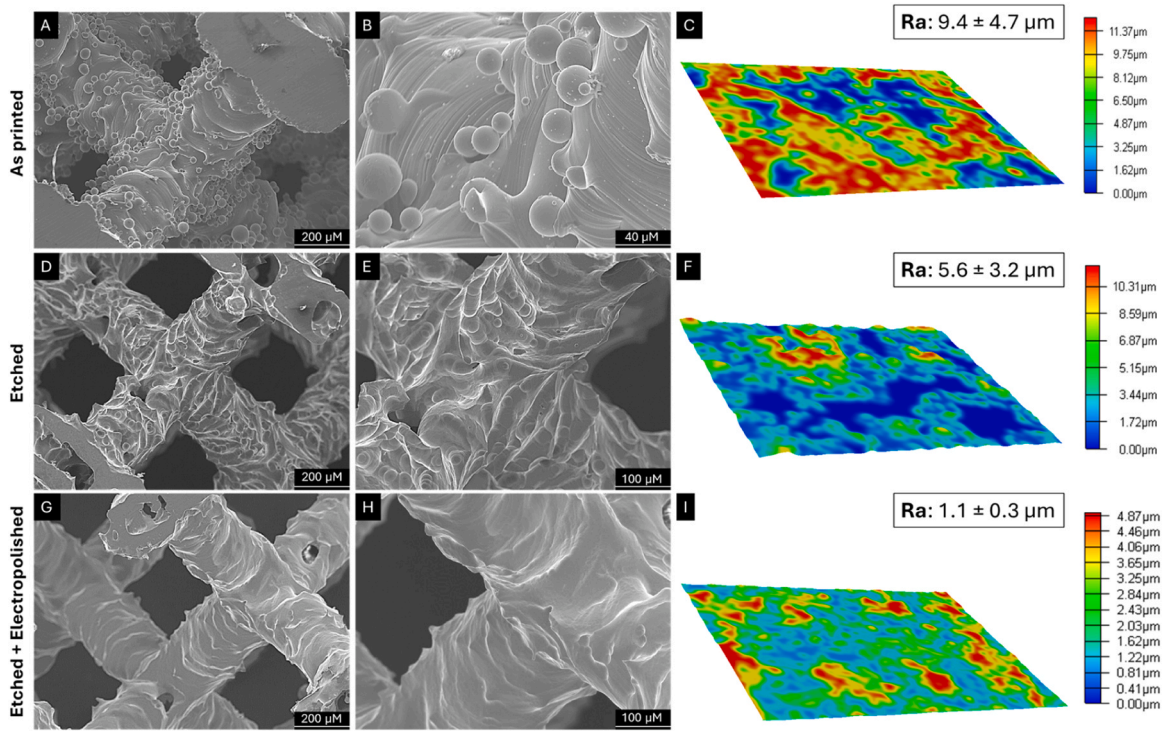

Fig. 3. Surface finishing and roughness of selected treatments analyzed by scanning electron micrographs and 3D topographic map of (A-C) as-printed, (D-F) etched (HNO_3/HF: 20/2.5 for 15 min), and (G-I) etched + electropolished (100 V for 2 min) LPBF Ti-6Al-4V scaffolds. The results are based on a sample size of n = 5 per condition and 10 measurements per sample.

3.2. Impact of surface treatment on LPBF Ti-6Al-4V scaffold surface properties

To assess how selected etching and combined etching-electropolishing treatments affect the surface morphology and material integrity of LPBF Ti-6Al-4V scaffolds, this section addresses the surface microstructure, topography, and roughness of the as-printed and surface-treated scaffolds (Fig. 3).

In the as-printed scaffold, the relatively high and random distribution of unmelted particles (Fig. 3A, B) accounts for its high roughness value (Fig. 3C), which is consistent with reported values in the literature for LPBF-printed Ti-6Al-4V alloys (5–40 μm) [38–40]. The presence of these particles results from direct contact with the surrounding powder bed from insufficient energy input and the need for an optimal combination of scanning speed, powder size, and layer height during printing [15,40]. However, the presence of unmelted particles is an inherent characteristic of MAM, as no study has reported a Ti-6Al-4V scaffold entirely free of them. There is thus a need for a surface post-treatment as a mandatory step to produce an implantable material since such particles have been reported to be released in physiological media, compromise cell attachment, increase the risk of bacterial colonization, and accelerate corrosion in physiological environments [29,41].

Concerning the etched scaffold (HNO_3/HF: 20/2.5 for 15 min), despite the nearly complete unmelted particle removal (Fig. 3D), some surface heterogeneities remained, such as sharp edges and relatively high roughness (Fig. 3E). Therefore, although the roughness of the scaffolds (Ra: arithmetic mean value in a roughness profile) was reduced by nearly 50 % compared to the as-printed scaffold (Fig. 3F), this value was comparable to the conventional HF etching (Ra: 3–6 μm) [42], but higher than combined acid etching (H_2SO_4/HCl/HF mixtures; Ra: 1.5–3 μm) for LPBF-printed Ti-6Al-4V scaffolds [42,43].

Notwithstanding, the etched + electropolished (100 V for 2 min) scaffold presented a uniform surface, free of unmelted particles with a similar mass loss to the etched scaffolds, *i.e.*, 27.5 vs. 25 wt%, respectively. Noticeably, its R_a value of 1 μm aligned with the typical standards for commercial titanium implants (R_a: 0.5–2.5 μm) [23]. This highlights the synergistic effect of both treatments.

High-resolution X-ray photoelectron spectroscopy (XPS) was performed to further analyze the composition of the oxide layer on the as-printed, etched, and etched + electropolished scaffolds. For relevance, Ti2p and O1s spectra were analyzed (Fig. 4).

The Ti2p spectra (highlighted in red in Fig. 4) reveal the presence of both metallic Ti and a TiO_2 passive layer in the as-printed and etched scaffolds. Besides, the presence of the Ti metal signal, although lower after etching, revealed that the TiO_2 oxide layer in these scaffolds was not thick or homogeneous enough [44,45].

In contrast, the etched + electropolished scaffold showed only TiO_2, with a slight increase in the intensity of the $Ti2p_{3/2}$ and $Ti2p_{1/2}$ peaks. This suggests that electropolishing promoted the formation of a thicker and more uniform oxide layer, effectively hampering the metallic Ti signal. This aligned with previous studies reporting that electropolishing enhances surface passivation and increases TiO_2 content by facilitating controlled oxidation of the Ti surface [44–46].

The O1s spectra confirmed the presence of TiO_2. In the as-printed and etched scaffolds, peak broadening around 531–535 eV corresponded to (i) adsorbed oxygen and hydroxyl (OH) groups from surface-bound water, and (ii) C-O bonding from the inherent contamination during scaffold manipulation [45,46]. Notably, in the etched + electropolished scaffold, the O1s peak was more intense and narrower, indicating a denser and more homogeneous oxide layer [46], as shown with the suppressed metallic Ti signal observed in the Ti2p spectrum.

PDP measurements in α-MEM on both the as-printed and etched + electropolished samples indicate passive current densities in the range of 10^{-7} – 10^{-8} A·cm^{-2}, consistent with the expected behaviour of Ti-6Al-4V alloy [47] (Figure S2). The as-printed specimens exhibited a markedly noisier and less stable response, likely due to their higher roughness and the presence of unmelted particles, which can act as local initiation sites for corrosion or detach during polarization. In contrast, the treated samples displayed a smoother polarization curve with a more stable passive region, indicative of a more homogeneous oxide layer. These results are in line with the discussed XPS results (Fig. 4). Given the complexity of accurately assessing corrosion in additively manufactured lattice structures and the need for more extensive and localized analyses, these results are provided only as a first approach in the Supporting Information (Figure S2). Nevertheless, other studies have evaluated the corrosion behaviour in additively manufactured Ti-6Al-4V more broadly and demonstrated a corrosion improvement after different surface treatments [48–50]. A full evaluation of electrochemical behaviour and corrosion mechanisms lies beyond the scope of this work and will be addressed in future studies.

3.3. Biocompatibility and cell growth in surface-treated Ti-6Al-4V scaffolds

After screening the surface treatments and selecting a protocol, the biocompatibility of the scaffolds was investigated to assess the possible effects of the presence of unmelted particles or any possible leached material into the medium. SCAP cells were seeded on Tissue Culture Plastic (TCP) wells, allowed to form a monolayer for 48 h, and then placed in contact with the titanium scaffolds (the scaffold was occupying less than 10 % of the total area) (Fig. 5A).

SCAP metabolic activity was similar for all the conditions (Fig. 5B), thus showing that all the scaffolds (as printed, etched, and etched + electropolished) were biocompatible, in agreement with the described properties of titanium alloys [51]. Increased viability was observed at 24 and 96 h, and a decrease in viability values was measured after 7 days for all the surface-modified scaffolds, without being statistically significant.

The cell monolayer that was in contact with the scaffolds was also followed over time (Fig. 5C), confirming its extension within the scaffold. Noteworthy, the etched + electropolished scaffold induced cell growth around the 3D printed structure, as denser areas of cells were found on the edges of the scaffold. Cells were then allowed to grow for 15 days scaffold, and their adhesion to the scaffold surface was assessed by fluorescent microscopy (Figure S3) and SEM (Fig. 5D).

As observed in SEM images, SCAP was able to form a monolayer on the etched + electropolished scaffold, while on the as-printed scaffolds, the cells adhered to the rough surface -including the unmelted particles- but were unable to grow to form a monolayer on the material. On the other hand, even though the etched scaffold showed a more uniform surface without the presence of unmelted particles, no cell monolayer was formed. Actin staining and GFP signal confirmed cell adhesion on all the scaffolds with elongated morphologies (Figure S3).

The enhanced surface growth observed in the etched + electropolished scaffold can be attributed to several factors. Firstly, its roughness value (Ra ~1 μm; Fig. 3) closely matched that of biomedical implant surfaces, particularly commercial dental implants, which typically present Ra values of 1–2 μm [23]. On the other hand, while orthopaedic implants can reach up to 100 μm, studies with mesenchymal stem cells (MSC) suggest that increased surface roughness may delay differentiation and extracellular matrix (ECM) formation, thus altering oxidative stress levels [52]. Also, a reduced roughness can benefit mammalian cell adhesion and a reduction in bacterial attachment [53], a key aspect when designing orthopaedic implants. Therefore, a smoother surface and a lower Ra value can be more beneficial for cell growth.

Secondly, the presence of a homogenous and thicker TiO_2 layer as a result of the electropolishing process, detected by XPS (Fig. 4), could allow better protein adsorption on the surface of the implants [54,55]. It would result in enhanced cell adhesion, as it has been found when the TiO_2 layer is formed by different techniques such as hydrothermal-,

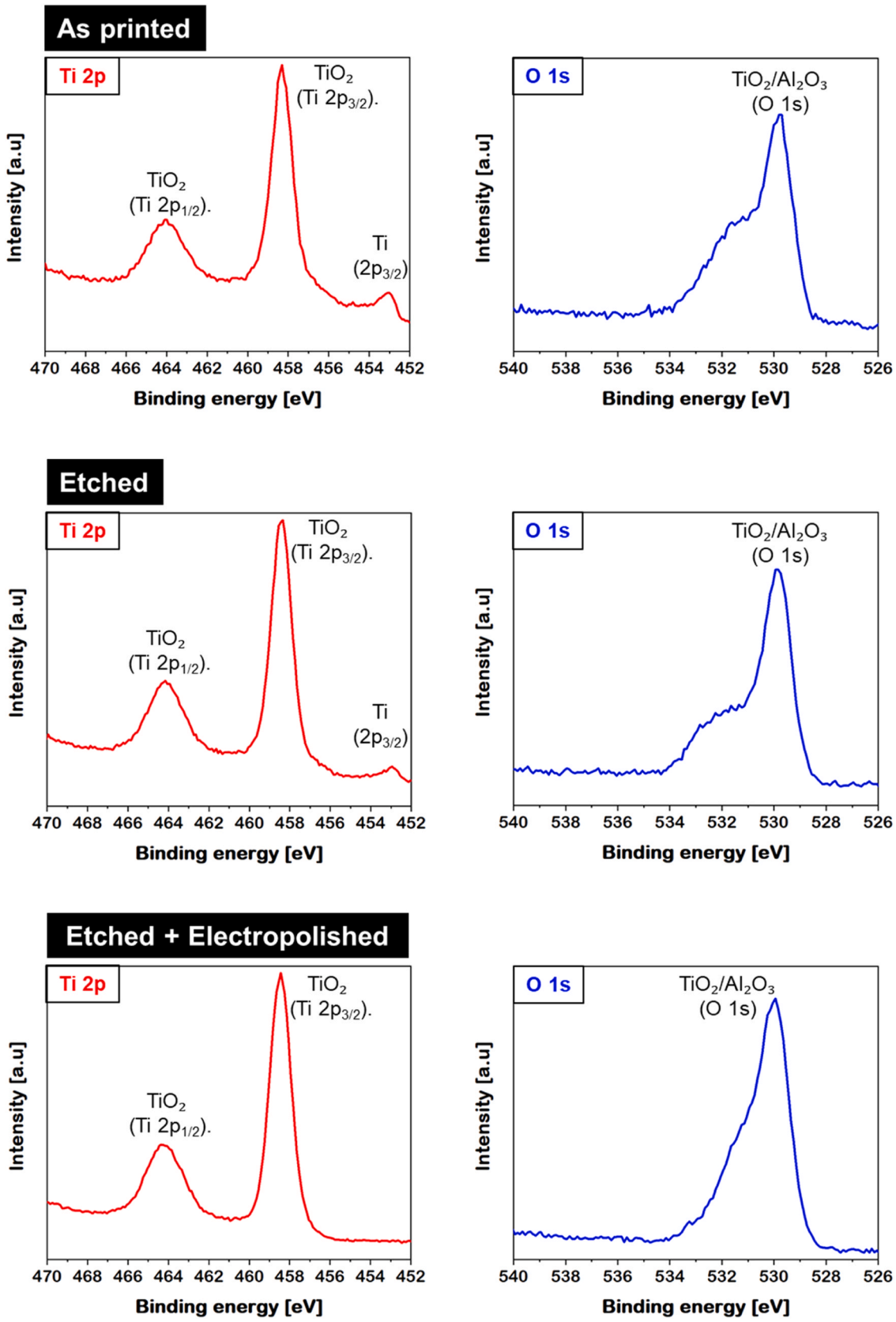

Fig. 4. Properties of the surface oxides by high-resolution XPS spectra of Ti 2p and O 1 s for as-printed, etched, and etched + electropolished LPBF-printed Ti-6Al-4V scaffolds. Note that Ti2p peak spectra were normalized with respect to the etched + electropolished scaffold.

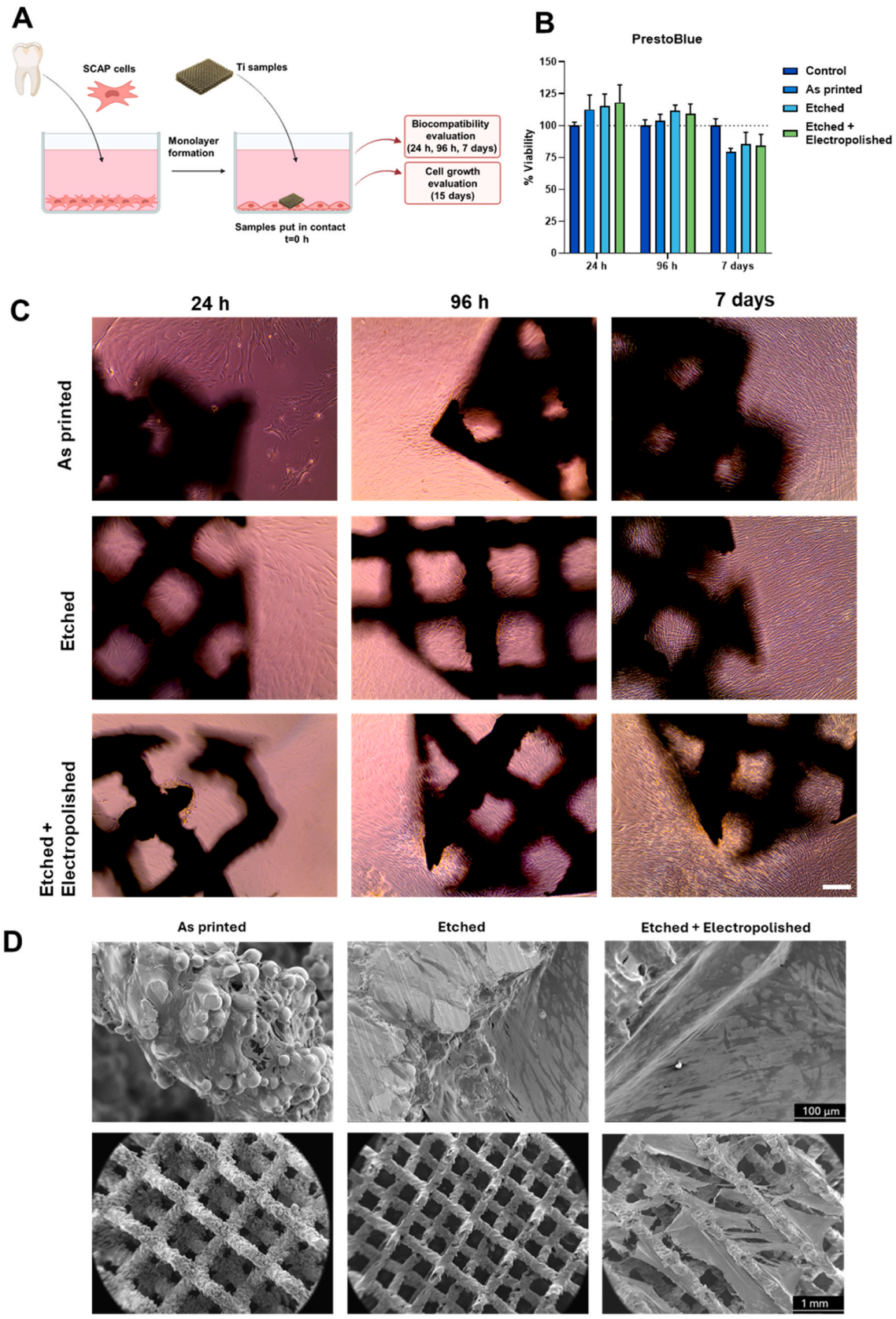

Fig. 5. Biocompatibility and growth evaluation of the materials with SCAP cells (A) Direct contact assay scheme, (B) Prestoblue assay after 24 h, 96 h, and 7 days of SCAP cells contact with the scaffolds (control plastic, as printed, etched, and etched + electropolished) represented considering 100 % viability of the control condition, (C) Wide-field microscopy images of growing SCAP in contact with the scaffolds at 24 h, 96 h, and 7 days; scale indicates 100 µm, and (D) SEM images at different magnifications of the cells growing on the materials after 15 days in contact. The results are based on a sample size of n = 4 per condition.

plasma-based treatments [56], anodizing and electrophoretic deposition [57], among others.

Given the results of the biocompatibility evaluation, the etched + electropolished scaffold was selected to further evaluate its impact on SCAP. The as-printed scaffold was used as a control. Fig. 6 shows live and dead assay of cells growing on the scaffolds after seeding on top. Very few cells in the as printed condition are positive for EthD-1 (dead marker), and most of the cells are alive (calcein positive in green). The treated condition presents all cells alive after 24 h and 96 h of seeding.

Fig. 7A shows the cell growth after the direct seeding into the materials at different time points (days 7, 14, 21, and 28), with a significant increase in their growth around the printed scaffolds. Although some rounded unmelted particles can be identified (marked as red in Fig. 7A), these particles can also be better identified in the well (Figure S4). The etched + electropolished scaffold showed a denser matrix of cells within the scaffold when compared to the as-printed condition (Fig. 7B).

This indicates that even though the base material was biocompatible and allowed cells to adhere and grow over it, the surface/structure was unstable, and the removal of the unmelted particles and unfinished structures before cell seeding, or implantation *in vivo,* is key to avoiding the leaching of unintended debris into the body. Whereas TiO_2 nanoparticles have been described to be neurotoxic [58], unmelted particles present a micrometric size, which makes cell uptake less efficient [41]. Nevertheless, these microparticles could end up accumulating in different tissues or organs *in vivo*. Studies with macrophages and different unmelted particle sizes (15–100 μm) and doses have determined that particle size and concentration modulate the resulting immune response [59]. Therefore, the removal of particles obtained by the surface treatment combination (etched + electropolished) could ensure the avoidance of an undesired immune response.

The study of SCAP gene expression after 28 days in contact within the material (Fig. 7C) showed differences in classic MSC markers such as CD90, CD73, and CD105 [30]. CD90 was over-expressed in the etched plus electropolished state, with significant differences compared to the other conditions. CD105 and CD73 were reduced when compared to the cells grown in T75 flasks (SCAP control). Nevertheless, marker expression in the etched + electropolished condition was higher compared to SCAP cells grown for 28 days on 2D (SCAP 28 days). Although a reduction in stemness markers is expected after prolonged time in culture, the priming effect- understood as how exposure to a specific stimulus influences a later response- of the scaffold may contribute to the preservation of the markers' expression. Whereas differentiation is increased in MSC with CD90 downregulation [60], highly expressing CD90 adipose-derived stromal cells have also been reported to exhibit enhanced osteogenic capacity at later stages [61].

CD73 and CD90 are highly expressed by MSC that present greater proliferation capacity *in vitro* [62]. This could explain why CD90 was increased in the etched plus electropolished condition, as more cells are found growing in comparison with the as printed condition. Nevertheless, by qPCR, we cannot individualize cell-by-cell expression of these surface markers to know the percentage of the population that remains positive; it only provides an overall expression level representative of the entire population.

The structure of 3D-printed porous materials has been reported to affect MSC differentiation [63]. SCAP can differentiate towards multiple lineages, including odontogenic and osteogenic [64], depending on the stimulus [65]. They can also modulate neuroinflammation [66]. Therefore, given the dental origin of the SCAP cells, the impact of scaffold surface treatment on osteogenesis/odontogenesis was also evaluated. Collagen I (Col1) and alkaline phosphatase (ALP) gene expression were highly upregulated after 28 days of culture in 2D compared to the control, indicating that after 1 month in culture, SCAP starts differentiation. Cells growing on the 3D-printed scaffolds, mainly in the as-printed condition, presented a lower expression than 2D cultured cells but still higher than the control. Runx2 gene expression, a major marker of osteogenic differentiation, was higher in the etched + electropolished condition compared to the control scaffold. This could be explained as Runx2 gene expression is higher at the early stage of osteogenic induction, then decreases during the differentiation process. This is key to osteoblast function maintenance, thus being undetectable when the osteocytes are formed [67]. Therefore, this gene can oscillate during the process, and it is difficult to assess these differences between scaffolds. Lastly, osteocalcin (OCN), a late differentiation marker, showed no significant differences between any of the samples, indicating there is no impact of the scaffold and treatment on late differentiation. Since no differentiation media or growth factor was used to induce osteo-differentiation, the resulting cultured cells could be a gradient of undifferentiated and differentiated cells. This could mirror what happens in their niche [68], as both stem cell markers and early-mid differentiation markers were found to be expressed. Strategies where there is an incorporation of an osteogenic agent (*i.e.*, BMP-2) within a polymeric coating have been explored in AM Ti scaffolds, showing an enhanced differentiation [69] and could provide a targeted therapeutic outcome.

To determine if the scaffolds were impacting SCAP immunological state, TSG6 gene expression was evaluated by RT-qPCR. TSG6 gene

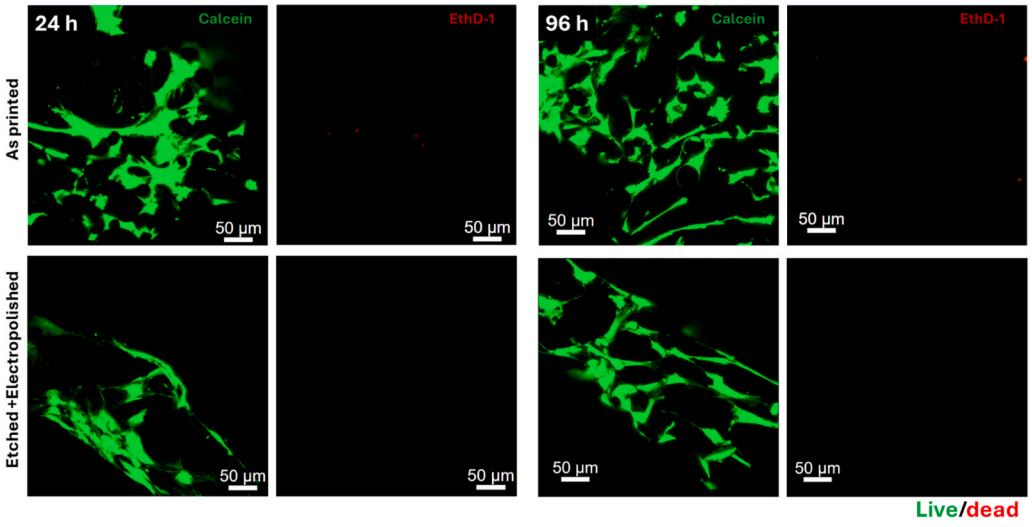

Fig. 6. Live and dead assay of SCAP cells after 24 h (left panel) and 96 h (right panel) of cell growth over the materials (as printed and etched+electropolished). Live cells in green (calcein) and dead cells in red (EthD-1).

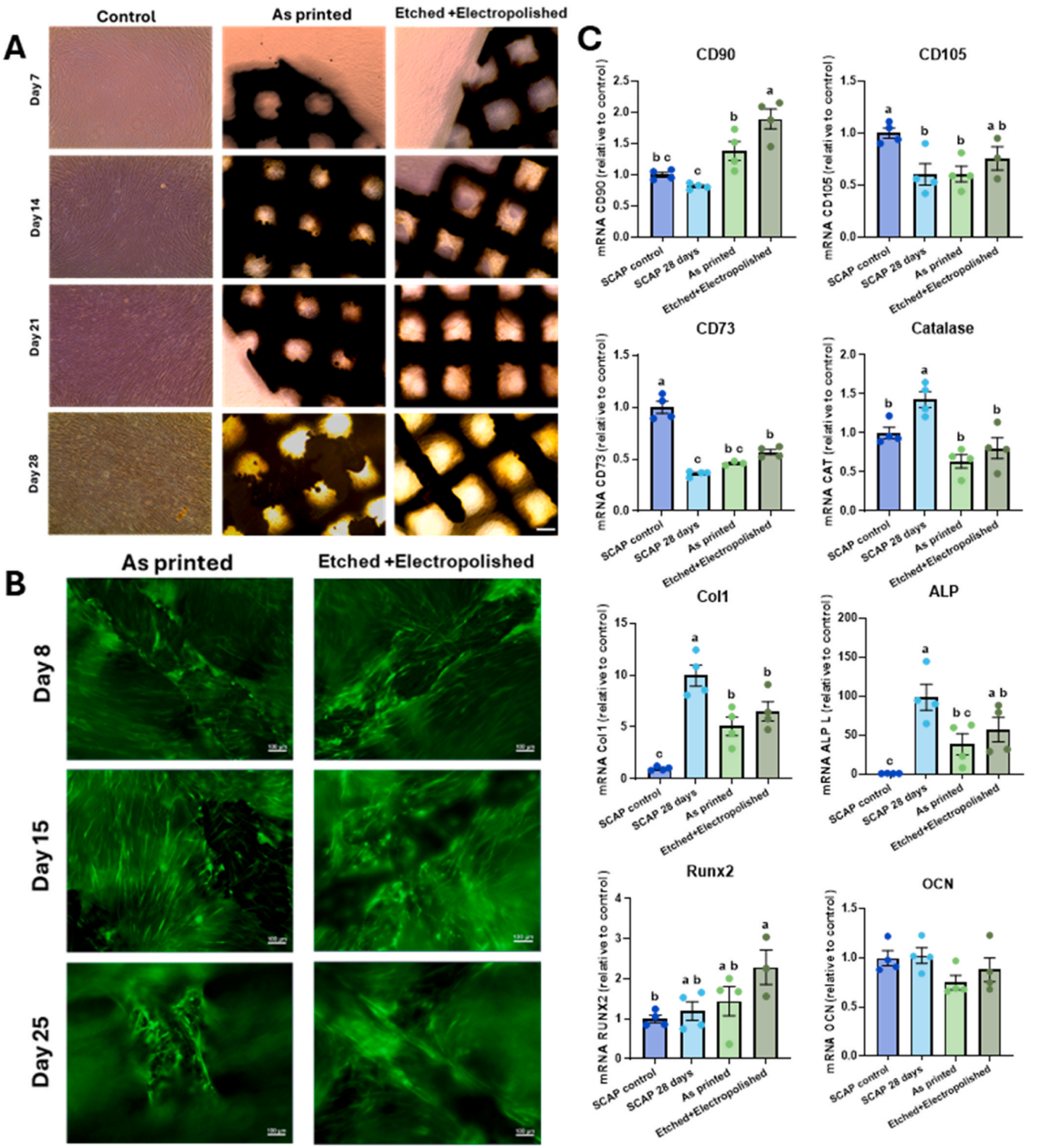

Fig. 7. Time overview of cell growth and gene expression evaluation in the control cells and cells growing over the scaffolds. (A) Wide-field microscopy images of growing SCAP on the plastic and Ti scaffolds (As printed and etched + electropolished) at 7, 14, 21, and 28 days; scale indicates 100 μm, (B) Fluorescent microscopy (GFP in green) of the adhered cells in as printed and etched + electropolished conditions at days 8, 15 and 25, and (C) mRNA expression of CD90, CD105, CD73, CAT (Catalase), Col1 (Collagen I), ALP L, RUNX2 and OCN after 28 days in culture of SCAP in plastic (SCAP 28 days), as printed and etched + electropolished compared to control SCAP. One-way ANOVA; mean ± SEM; n = 4. Significant differences between groups are displayed by CLD, where a different letter (a,b, and c) indicates that both groups are statistically different.

expression increased in the cells growing in 2D after 28 days of culture (Figure S5), but not on either of the scaffolds. Taken together, this could indicate that SCAP maintained on the materials for 28 days do not exhibit signs of immunological activation.

Lastly, to explore the impact of potential leaching materials on oxidative stress, the gene expression of catalase was evaluated (Fig. 7C). It was significantly lower when SCAP grew on the scaffolds compared to 2D culture, with no impact of surface treatment. Nevertheless, in order

to know the possible oxidative stress on the first 24 h in contact, where more leached particles could be expected, a ROS assay with murine macrophages was performed (Fig. 8). The results indicate that the materials and their leached debris do not induce oxidative stress after 24 h.

Fig. 9A shows how SCAP seeded on etched + electropolished scaffolds formed a more uniform and continuous tissue-like structure. Also, visible calcium deposits were not detected by SEM in either of the scaffolds, which could indicate an earlier state of differentiation, as corroborated by PCR results with no increase in OCN levels. Mineralization can be considered the last stage of osteogenic differentiation.

To sum up, scaffold-shaped Ti-6Al-4V alloy allows cells to grow within the structure could improve their implantation success for prosthesis applications. Either by preseeding cells before implantation, such as SCAP in this work, or by allowing the patient's cells to reach the inner structure of the implant and colonize it after implantation, new bone within the biomaterial could be obtained. Likewise, considering the current findings, it can be stated that not only the implant geometry but also the surface modification of these materials can impact the implant's outcome.

In this scenario, note that most commercial surface treatments to enhance Ti alloy biocompatibility - machining (Brånemark Standard), sandblasting (OsseoSpeed®, TiOblast), double acid-etching (Osseotite®), electrochemical methods like anodization, and bioactive coatings (Biomimetic®) - have been primarily evaluated on conventionally manufactured Ti alloys, not on MAM-processed Ti alloys [23,70–72]. While these approaches improve certain surface or cellular responses, the combination of chemical etching and electropolishing in this study provides a clear advantage for LPBF-produced complex geometries, offering uniform surface topography and removal of unmelted particles. Also, we can state that SCAP cells remained viable on the treated surfaces and formed a tissue-like matrix by day 28, maintaining stem cell markers, increasing early-mid osteogenic markers, and showing no oxidative stress, demonstrating a supportive environment for cell growth and differentiation.

4. Conclusions and future outlook

This study successfully demonstrated, for the first time, the effective combination of etching and electropolishing treatments on LPBF-printed Ti-6Al-4V to reduce surface roughness and defects such as unmelted powder particles, and to promote the formation of a uniform TiO_2 layer, thereby improving the implantability of the alloy. The main conclusions regarding surface finishing and biocompatibility can be summarized as follows:

- **Surface finishing**: Among the studied etching conditions, immersion of the Ti-6Al-4V scaffold in HNO_3/HF: 20.0/2.2 solution for 15 min effectively removed the unmelted particles. On the other hand, electropolishing treatment, especially at 100 V for 2 min, improves surface smoothness but does not remove the presence of unmelted particles. However, microstructural analysis revealed that the combination of both selected treatments significantly reduced the surface roughness (OM, SEM), favoring the formation of a thicker and more homogeneous TiO_2 layer (XPS).
- ***In vitro* evaluation**: 3D printed materials were biocompatible both as printed and etched + electropolished combination after 7 days of culture. Notwithstanding, compared to the as-printed scaffold, the etched + electropolished scaffolds allowed the adhesion and

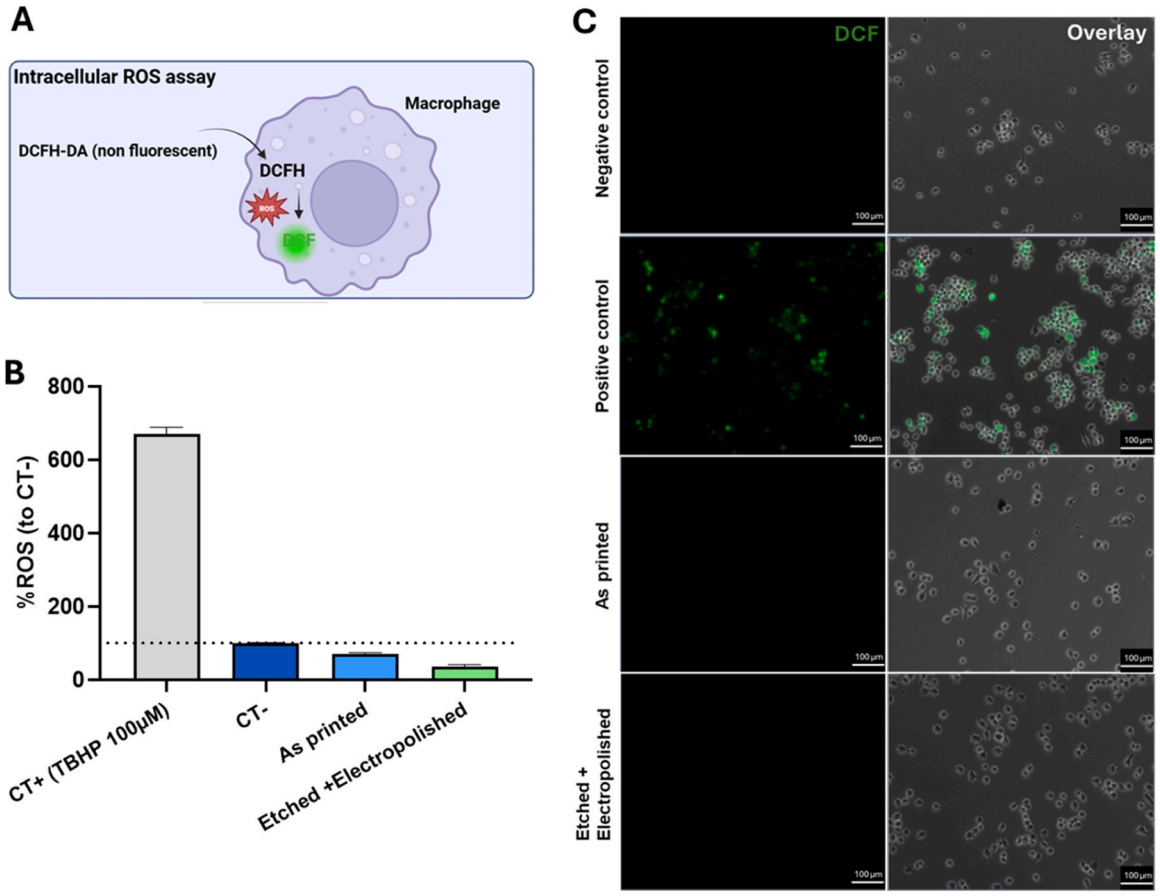

Fig. 8. Oxidative stress evaluation in murine macrophages (RAW 264.7) after 24 h in contact. (A) Intracellular ROS assay mechanism scheme (made with BioRender) (B) ROS quantification of positive control (CT+; treated with TBHP 100 μM), negative control (C-; seeded cells without any addition), cells in contact with as-printed sample or etched+electropolished sample. (C) Microscopy images of the DCF signal in green and overlay of bright field and DCF, scale bar 100 μm. n = 4.

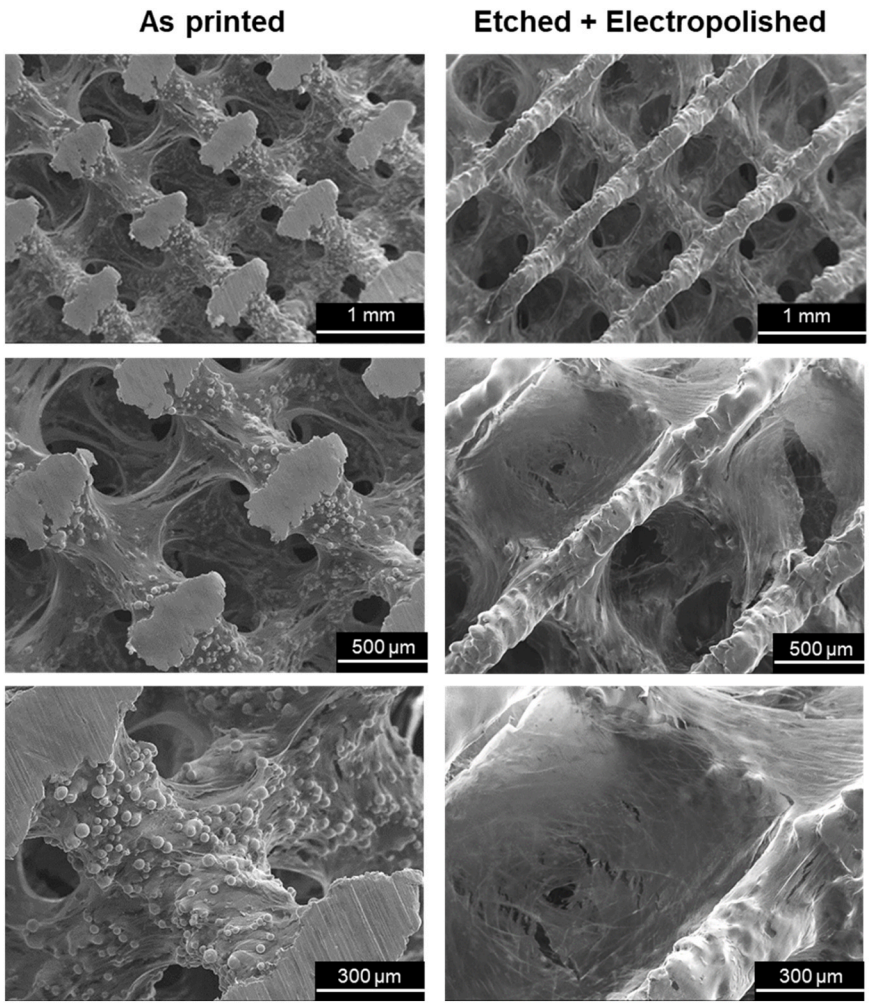

Fig. 9. Long-term growth of SCAP cells in the scaffolds. SEM images at different magnifications of SCAP cells growing on the materials (As printed and etched + electropolished) after 28 days.

monolayer formation of SCAP after 15 days. When seeded on top, cells were alive after 96 h in both samples. Moreover, when seeded on and left to grow for 28 days, SCAP formed a tissue-like structure with increased expression of CD90, conserved expression of CD73 and CD105, and positive expression of osteogenic differentiation markers (Col1, ALP, and Runx2) but no late differentiation (OCN). Moreover, oxidative stress, evaluated by catalase expression and ROS assay, confirmed that the Ti-6Al-4V was non-toxic after four weeks or 24 h, respectively. These findings highlight the advantages of applying combined surface treatments, which effectively removed unmelted particles - known to negatively impact cell response and surface integrity - while improving both surface finish and implantability of 3D-printed Ti alloys.

Given the obtained results, in the future, other approaches could be implemented, such as i) functionalization of the etched + electropolished 3D-printed scaffolds to directly guide the differentiation; ii) coating the etched + electropolished scaffold with a drug-loaded hydrogel to obtain a drug delivery system; iii) encapsulating cells into a hydrogel to ensure a homogeneous growth within the 3D structure.

Another aspect to study is the corrosion evaluation of the treated titanium surfaces. While the available literature approaches vary widely in medium composition and methodology, there is still a lack of systematic study of corrosion mechanisms and long-term stability of complex-shaped Ti alloys in biologically realistic conditions.

In light of the present findings, the proposed surface treatment approach could be further applied to other additively manufactured Ti-based alloys and geometries, offering a versatile strategy for eliminating unmelted particles and enhancing implant surface finishing and implantability. Besides, in larger structures, some degree of process optimization may be required, particularly during electropolishing, where current distribution and mass transport become more critical. The etching step, however, is expected to remain highly effective, as the electrolyte can easily access the entire surface and efficiently remove unmelted particles. Therefore, the possible process optimization for larger implants may include longer treatment times and, eventually, increased electrolyte agitation, temperature control, or pulsed potentials.

CRediT authorship contribution statement

Ana Santos-Coquillat: Writing – review & editing, Writing – original draft, Visualization, Validation, Software, Project administration, Methodology, Investigation, Funding acquisition, Formal analysis, Data curation, Conceptualization. **Iris De Graeve:** Writing – review & editing, Resources, Project administration, Funding acquisition. **Anne des Rieux:** Writing – review & editing, Resources, Project administration, Funding acquisition. **Brecht Van Hooreweder:** Writing – review & editing, Resources. **Kitty Baert:** Methodology, Formal analysis, Data curation. **Floriane Debuisson:** Writing – review & editing, Methodology, Formal analysis. **Revilla Reynier:** Writing – review & editing,

Visualization, Formal analysis. **Del Olmo Martinez Ruben:** Writing – review & editing, Writing – original draft, Visualization, Validation, Software, Project administration, Methodology, Investigation, Funding acquisition, Formal analysis, Data curation, Conceptualization.

Declaration of Competing Interest

The authors declare that they have no known competing financial interests or personal relationships that could have appeared to influence the work reported in this paper.

Acknowledgments

Rubén del Olmo acknowledges Marie Skłodowska-Curie Postdoctoral Fellowship (MSCA-PF), grant ID 101066947-EU651 project. Ana Santos-Coquillat is grateful for financial support from Fonds de la Recherche Scientifique (F.R.S.-FNRS) as Chargée de recherches. All the authors acknowledge Bart Lippens and Priya Laha from the MACH department of the VUB for their contribution to the scaffold preparation and valuable input to cell characterization by SEM, respectively. All the authors acknowledge Marie Auquière from UCLouvain for her contribution with mRNA extraction.

Appendix A. Supporting information

Supplementary data associated with this article can be found in the online version at doi:10.1016/j.addma.2026.105083.

Data availability

Data will be made available on request.

References

[1] E.Rezvani Ghomi, F. Khosravi, R.E. Neisiany, S. Singh, S. Ramakrishna, Future of additive manufacturing in healthcare, Curr. Opin. Biomed. Eng. 17 (2021) 100255.
[2] A.A. Zadpoor, Design for additive bio-manufacturing: from patient-specific medical devices to rationally designed meta-biomaterials, Int. J. Mol. Sci. 18 (8) (2017).
[3] J. Ping, C. Zhou, Y. Dong, X. Wu, X. Huang, B. Sun, B. Zeng, F. Xu, W. Liang, Modulating immune microenvironment during bone repair using biomaterials: focusing on the role of macrophages, Mol. Immunol. 138 (2021) 110–120.
[4] S.S. Sidhu, H. Singh, M.A.-H. Gepreel, A review on alloy design, biological response, and strengthening of β-titanium alloys as biomaterials, Mater. Sci. Eng. C 121 (2021) 111661.
[5] M.H. Razzaq, M.U. Zaheer, H. Asghar, O.C. Aktas, M.F. Aycan, Y.K. Mishra, Additive manufacturing for biomedical bone implants: shaping the future of bones, Mater. Sci. Eng. R Rep. 163 (2025) 100931.
[6] Y. Yang, S. Yan, S. Qu, M. Yi, Z. Chen, T. Zhou, C. Xu, Microstructure of titanium alloy in additive/subtractive hybrid manufacturing: a review, J. Alloy. Compd. 1014 (2025) 178769.
[7] R. del Olmo, E. Martínez-Campos, J.J. Relinque, A. Gallardo, J. Rodríguez-Hernández, E. Matykina, A. Santos-Coquillat, in: S.J. Ikhmayies (Ed.), New Trends in the Design of Biomaterials for 3D and 4D Printing, Advances in Biomaterials Research, Springer Nature Switzerland, Cham, 2025, pp. 57–119.
[8] J. Li, H. Fan, H. Li, L. Hua, J. Du, Y. He, Y. Jin, Recent advancements in the surface modification of additively manufactured metallic bone implants, Addit. Manuf. Front. 4 (1) (2025) 200195.
[9] J.D. Avila, S. Bose, A. Bandyopadhyay, 3.7 - Additive manufacturing of titanium and titanium alloys for biomedical applications, in: F.H. Froes, M. Qian (Eds.), Titanium in Medical and Dental Applications, Woodhead Publishing, 2018, pp. 325–343.
[10] A. Leon, G.K. Levy, T. Ron, A. Shirizly, E. Aghion, The effect of hot isostatic pressure on the corrosion performance of Ti-6Al-4 V produced by an electron-beam melting additive manufacturing process, Addit. Manuf. 33 (2020) 101039.
[11] R. Ramakrishnaiah, A.A. Al kheraif, A. Mohammad, D.D. Divakar, S.B. Kotha, S. L. Celur, M.I. Hashem, P.K. Vallittu, I.U. Rehman, Preliminary fabrication and characterization of electron beam melted Ti–6Al–4V customized dental implant, Saudi J. Biol. Sci. 24 (4) (2017) 787–796.
[12] A. Bandyopadhyay, I. Mitra, A. Shivaram, N. Dasgupta, S. Bose, Direct comparison of additively manufactured porous titanium and tantalum implants towards in vivo osseointegration, Addit. Manuf. 28 (2019) 259–266.
[13] A. Bandyopadhyay, A. Shivaram, S. Tarafder, H. Sahasrabudhe, D. Banerjee, S. Bose, In vivo response of laser processed porous titanium implants for load-bearing implants, Ann. Biomed. Eng. 45 (1) (2017) 249–260.
[14] Y. Li, C. Liu, J. Gu, M. Song, Recent advances on defects, microstructures and mechanical properties of additively manufactured titanium alloys, Mater. Today Commun. 42 (2025) 111312.
[15] H.Y. Ma, J.C. Wang, P. Qin, Y.J. Liu, L.Y. Chen, L.Q. Wang, L.C. Zhang, Advances in additively manufactured titanium alloys by powder bed fusion and directed energy deposition: microstructure, defects, and mechanical behavior, J. Mater. Sci. Technol. 183 (2024) 32–62.
[16] C. O'Keeffe, D. Taylor, C. Lally, D.J. Kelly, Morphological induced improvements in the bulk mechanical properties of chemically etched additively manufactured Ti-6Al-4V micro-struts, Addit. Manuf. 75 (2023) 103748.
[17] L. Thijs, F. Verhaeghe, T. Craeghs, J.V. Humbeeck, J.-P. Kruth, A study of the microstructural evolution during selective laser melting of Ti–6Al–4V, Acta Mater. 58 (9) (2010) 3303–3312.
[18] H. Masuo, Y. Tanaka, S. Morokoshi, H. Yagura, T. Uchida, Y. Yamamoto, Y. Murakami, Influence of defects, surface roughness and HIP on the fatigue strength of Ti-6Al-4V manufactured by additive manufacturing, Int. J. Fatigue 117 (2018) 163–179.
[19] H. Masuo, Y. Tanaka, S. Morokoshi, H. Yagura, T. Uchida, Y. Yamamoto, Y. Murakami, Effects of defects, surface roughness and HIP on fatigue strength of Ti-6Al-4V manufactured by additive manufacturing, Procedia Struct. Integr. (2017) 19–26.
[20] S.A. Tyagi, M. M, Additive manufacturing of titanium-based lattice structures for medical applications – a review, Bioprinting 30 (2023) e00267.
[21] V.M.S. Muthaiah, S. Indrakumar, S. Suwas, K. Chatterjee, Surface engineering of additively manufactured titanium alloys for enhanced clinical performance of biomedical implants: a review of recent developments, Bioprinting 25 (2022) e00180.
[22] M.M. Basha, S.M. Basha, V.K. Jain, M.R. Sankar, State of the art on chemical and electrochemical based finishing processes for additive manufactured features, Addit. Manuf. 58 (2022) 103028.
[23] R. del Olmo, M. Czerwiński, A. Santos-Coquillat, V. Dubey, S.J. Dhoble, M. Michalska-Domańska, Nano-scale Surface Modification of Dental Implants: Fabrication, in: K. Gulati (Ed.), Surface Modification of Titanium Dental Implants, Springer International Publishing, Cham, 2023, pp. 83–116.
[24] R.N. Oosterbeek, G. Sirbu, S. Hansal, K. Nai, J.R.T. Jeffers, Effect of chemical–electrochemical surface treatment on the roughness and fatigue performance of porous titanium lattice structures, Addit. Manuf. 78 (2023) 103896.
[25] A. Acquesta, T. Monetta, The electropolishing of additively manufactured parts in titanium: state of the art, Adv. Eng. Mater. 23 (12) (2021) 2100545.
[26] A. Acquesta, T. Monetta, S. Franchitti, R. Borrelli, A. Viscusi, A.S. Perna, F. Penta, L. Esposito, L. Carrino, Green electrochemical polishing of EBM Ti6Al4V samples with preliminary fatigue results, Int. J. Adv. Manuf. Technol. 126 (9) (2023) 4269–4282.
[27] A.N. Aufa, M.Z. Hassan, Z. Ismail, Recent advances in Ti-6Al-4V additively manufactured by selective laser melting for biomedical implants: prospect development, J. Alloy. Compd. 896 (2022) 163072.
[28] E.M.M. Sutter, G.J. Goetz-Grandmont, The behaviour of titanium in nitric-hydrofluoric acid solutions, Corros. Sci. 30 (4) (1990) 461–476.
[29] B. Wysocki, J. Idaszek, J. Buhagiar, K. Szlązak, T. Brynk, K.J. Kurzydłowski, The influence of chemical polishing of titanium scaffolds on their mechanical strength and in-vitro cell response, Materials Science Engineering C 95 (2019) 428–439.
[30] N.B. Ruparel, J.F. de Almeida, M.A. Henry, A. Diogenes, Characterization of a stem cell of apical papilla cell line: effect of passage on cellular phenotype, J. Endod. 39 (3) (2013) 357–363.
[31] A. Follenzi, L.E. Ailles, S. Bakovic, M. Geuna, L. Naldini, Gene transfer by lentiviral vectors is limited by nuclear translocation and rescued by HIV-1 pol sequences, Nat. Genet. 25 (2) (2000) 217–222.
[32] F. Debuisson, B. Ucakar, K. Vanvarenberg, K.-A. Delongie, V. Haufroid, A. Mwema, A. des Rieux, Nanomedicine-enhanced SCAP hybrid spheroids: a novel approach for improved stem cell survival, Int. J. Pharm. 675 (2025) 125503.
[33] B. Lizcano-Perret, C. Lardinois, F. Wavreil, P. Hauchamps, G. Herinckx, F. Sorgeloos, D. Vertommen, L. Gatto, T. Michiels, Cardiovirus leader proteins retarget RSK kinases toward alternative substrates to perturb nucleocytoplasmic traffic, PLoS Pathog. 18 (12) (2022) e1011042.
[34] H. Lee, H.-D. Jung, M.-H. Kang, J. Song, H.-E. Kim, T.-S. Jang, Effect of HF/HNO3-treatment on the porous structure and cell penetrability of titanium (Ti) scaffold, Mater. Des. 145 (2018) 65–73.
[35] F. Scherillo, E. Manco, A.E. Hassanin, S. Franchitti, C. Pirozzi, R. Borrelli, Chemical surface finishing of electron beam melted Ti6Al4V using HF-HNO3 solutions, J. Manuf. Process. 60 (2020) 400–409.
[36] L. Skowronski, M. Chorobinski, The effect of thickness and optical constants of the dielectric layer on the color behaviour of the glass/Ti/TiO2 decorative coatings, Thin Solid Films 691 (2019) 137595.
[37] D. Kim, K. Son, D. Sung, Y. Kim, W. Chung, Effect of added ethanol in ethylene glycol–NaCl electrolyte on titanium electropolishing, Corros. Sci. 98 (2015) 494–499.
[38] K.S. Chan, M. Koike, R.L. Mason, T. Okabe, Fatigue life of titanium alloys fabricated by additive layer manufacturing techniques for dental implants, Metall. Mater. Trans. A 44 (2) (2013) 1010–1022.
[39] P. Edwards, M. Ramulu, Fatigue performance evaluation of selective laser melted Ti–6Al–4V, Materials Science Engineering A 598 (2014) 327–337.
[40] S. Liu, Y.C. Shin, Additive manufacturing of Ti6Al4V alloy: a review, Mater. Des. 164 (2019) 107552.

[41] X. He, E. Hartlieb, L. Rothmund, J. Waschke, X. Wu, K.L. Van Landuyt, S. Milz, B. Michalke, R. Hickel, F.-X. Reichl, C. Högg, Intracellular uptake and toxicity of three different Titanium particles, Dent. Mater. 31 (6) (2015) 734–744.
[42] J. Kónya, H. Jaber, T.A. Kovács, H. Hargitai, Effects of selective laser melting building directions and surface modifications on surface roughness of Ti6Al4V alloy, Discov. Appl. Sci. 6 (1) (2024) 5.
[43] A.N. Aufa, M.Z. Hassan, Z. Ismail, N. Harun, J. Ren, M.F. Sadali, Surface enhancement of Ti–6Al–4V fabricated by selective laser melting on bone-like apatite formation, J. Mater. Res. Technol. 19 (2022) 4018–4030.
[44] V.V. Atuchin, V.G. Kesler, N.V. Pervukhina, Z. Zhang, Ti 2p and O 1s core levels and chemical bonding in titanium-bearing oxides, J. Electron Spectrosc. Relat. Phenom. 152 (1) (2006) 18–24.
[45] L. Mohan, S. Kar, P.S. Mahapatra, M. Nagai, T.S. Santra, Fabrication of TiO2 microspikes for highly efficient intracellular delivery by pulse laser-assisted photoporation, RSC Adv. 11 (16) (2021) 9336–9348.
[46] C. Anandan, L. Mohan, In vitro corrosion behavior and apatite growth of oxygen plasma ion implanted titanium alloy β-21S, J. Mater. Eng. Perform. 22 (11) (2013) 3507–3516.
[47] X. Zhou, D. Xu, S. Geng, Y. Fan, C. Yang, Q. Wang, F. Wang, Microstructural evolution and corrosion behavior of Ti–6Al–4V alloy fabricated by laser metal deposition for dental applications, J. Mater. Res. Technol. 14 (2021) 1459–1472.
[48] C. García-Hernández, C. García-Cabezón, F. González-Diez, M. Ampudia, D. Juanes-Gusano, J.C. Rodriguez-Cabello, F. Martín-Pedrosa, Effect of processing on microstructure, mechanical properties, corrosion and biocompatibility of additive manufacturing Ti-6Al-4V orthopaedic implants, Sci. Rep. 15 (1) (2025) 14087.
[49] D. Gürkan, B. Sagbas, D. Uzunsoy, B. Dalbayrak, E.D. Arisan, A comparative study about corrosion resistance and biocompatibility of Ti6Al4V samples produced by wrought and additive manufacturing methods, Mater. Chem. Phys. 347 (2026) 131503.
[50] D. Pupillo, F.Di Franco, D. Palmeri, G. Pollara, G. Buffa, L. Fratini, M. Santamaria, Surface treatments on 3D printed Ti6Al4V biomedical plates to enhance corrosion resistance in simulated physiological solutions and under inflammatory conditions, Corros. Sci. 240 (2024) 112451.
[51] T. Hanawa, Biocompatibility of titanium from the viewpoint of its surface, Sci. Technol. Adv. Mater. 23 (1) (2022) 457–472.
[52] E.A. Lewallen, W.H. Trousdale, R. Thaler, J.J. Yao, W. Xu, J.M. Denbeigh, A. Nair, J.P. Kocher, A. Dudakovic, D.J. Berry, R.C. Cohen, M.P. Abdel, D.G. Lewallen, A. J. van Wijnen, Surface roughness of titanium orthopedic implants alters the biological phenotype of human mesenchymal stromal cells, Tissue Eng. Part A 27 (23-24) (2021) 1503–1516.
[53] V.M. Villapún, L.N. Carter, N. Gao, O. Addison, M.A. Webber, D.E.T. Shepherd, J. W. Andrews, M. Lowther, S. Avery, S.J. Glanvill, L.M. Grover, S. Cox, A design approach to facilitate selective attachment of bacteria and mammalian cells to additively manufactured implants, Addit. Manuf. 36 (2020) 101528.
[54] B.E. Rapuano, J.J.E. Lee, D.E. MacDonald, Titanium alloy surface oxide modulates the conformation of adsorbed fibronectin to enhance its binding to α5β1 integrins in osteoblasts, Eur. J. Oral. Sci. 120 (3) (2012) 185–194.
[55] S.R. Sousa, M. Lamghari, P. Sampaio, P. Moradas-Ferreira, M.A. Barbosa, Osteoblast adhesion and morphology on TiO2 depends on the competitive preadsorption of albumin and fibronectin, J. Biomed. Mater. Res. Part A 84 (2) (2008) 281–290.
[56] M.R. Mahbub, L. Kovach, A. Wolfe, S. Lalvani, P.F. James, M.P. Jahan, Enhancing cell adhesion and corrosion performance of titanium alloy by surface and sub-surface engineering using WEDM, Surf. Coat. Technol. 429 (2022) 127929.
[57] Y.-J. Wu, C.-Y. Wang, H. Mana-ay, C.-S. Tu, P.-L. Lai, P.-Y. Chen, Achieving high surface bioactivity and adhesion in Ti-6Al-4V alloy via anodic oxidation and electrophoretic deposition, Ceramics International (2025).
[58] M. Czajka, K. Sawicki, K. Sikorska, S. Popek, M. Kruszewski, L. Kapka-Skrzypczak, Toxicity of titanium dioxide nanoparticles in central nervous system, Toxicol. Vitro Int. J. Published Assoc. BIBRA 29 (5) (2015) 1042–1052.
[59] J.C. Tang, J.P. Luo, Y.J. Huang, J.F. Sun, Z.Y. Zhu, J.Y. Xu, M.S. Dargusch, M. Yan, Immunological response triggered by metallic 3D printing powders, Addit. Manuf. 35 (2020) 101392.
[60] D.A. Moraes, T.T. Sibov, L.F. Pavon, P.Q. Alvim, R.S. Bonadio, J.R. Da Silva, A. Pic-Taylor, O.A. Toledo, L.C. Marti, R.B. Azevedo, D.M. Oliveira, A reduction in CD90 (THY-1) expression results in increased differentiation of mesenchymal stromal cells, Stem Cell Res. Ther. 7 (1) (2016) 97.
[61] M.T. Chung, C. Liu, J.S. Hyun, D.D. Lo, D.T. Montoro, M. Hasegawa, S. Li, M. Sorkin, R. Rennert, M. Keeney, F. Yang, N. Quarto, M.T. Longaker, D.C. Wan, CD90 (Thy-1)-positive selection enhances osteogenic capacity of human adipose-derived stromal cells, Tissue Eng. Part A 19 (7-8) (2013) 989–997.
[62] Y. Cao, A.L. Boss, S.M. Bolam, J.T. Munro, H. Crawford, N. Dalbeth, R.C. Poulsen, B.G. Matthews, In vitro cell surface marker expression on mesenchymal stem cell cultures does not reflect their ex vivo phenotype, Stem Cell Rev. Rep. 20 (6) (2024) 1656–1666.
[63] K.M. Ferlin, M.E. Prendergast, M.L. Miller, D.S. Kaplan, J.P. Fisher, Influence of 3D printed porous architecture on mesenchymal stem cell enrichment and differentiation, Acta Biomater. 32 (2016) 161–169.
[64] Q. Liu, Y. Gao, J. He, Stem cells from the apical papilla (SCAPs): past, present, prospects, and challenges, Biomedicines 11 (7) (2023) 2047.
[65] J. Vanacker, A. Viswanath, P. De Berdt, A. Everard, P.D. Cani, C. Bouzin, O. Feron, A. Diogenes, J.G. Leprince, A. des Rieux, Hypoxia modulates the differentiation potential of stem cells of the apical papilla, J. Endod. 40 (9) (2014) 1410–1418.
[66] P. De Berdt, P. Bottemanne, J. Bianco, M. Alhouayek, A. Diogenes, A. Lloyd, A. Llyod, J. Gerardo-Nava, G.A. Brook, V. Miron, G.G. Muccioli, A.D. Rieux, Stem cells from human apical papilla decrease neuro-inflammation and stimulate oligodendrocyte progenitor differentiation via activin-A secretion, Cell. Mol. life Sci. CMLS 75 (15) (2018) 2843–2856.
[67] J. Xu, Z. Li, Y. Hou, W. Fang, Potential mechanisms underlying the Runx2 induced osteogenesis of bone marrow mesenchymal stem cells, Am. J. Transl. Res. 7 (12) (2015) 2527–2535.
[68] H. Donnelly, M. Salmeron-Sanchez, M.J. Dalby, Designing stem cell niches for differentiation and self-renewal, J. R. Soc. Interface 15 (145) (2018).
[69] S. Amin Yavari, M. Croes, B. Akhavan, F. Jahanmard, C.C. Eigenhuis, S. Dadbakhsh, H.C. Vogely, M.M. Bilek, A.C. Fluit, C.H.E. Boel, B.C.H. van der Wal, T. Vermonden, H. Weinans, A.A. Zadpoor, Layer by layer coating for bio-functionalization of additively manufactured meta-biomaterials, Addit. Manuf. 32 (2020) 100991.
[70] H. De Bruyn, V. Christiaens, R. Doornewaard, M. Jacobsson, J. Cosyn, W. Jacquet, S. Vervaeke, Implant surface roughness and patient factors on long-term peri-implant bone loss, 2000, Periodontology 73 (1) (2017) 218–227.
[71] F. Jordana, L. Susbielles, J. Colat-Parros, Periimplantitis and implant body roughness: a systematic review of literature, Implant Dent. 27 (6) (2018) 672–681.
[72] A.I. Nicolas-Silvente, E. Velasco-Ortega, I. Ortiz-Garcia, L. Monsalve-Guil, J. Gil, A. Jimenez-Guerra, Influence of the titanium implant surface treatment on the surface roughness and chemical composition 13 (2) (2020) 314.